Kinoshita et al., https://doi.org/10.1083/jcb.201607086

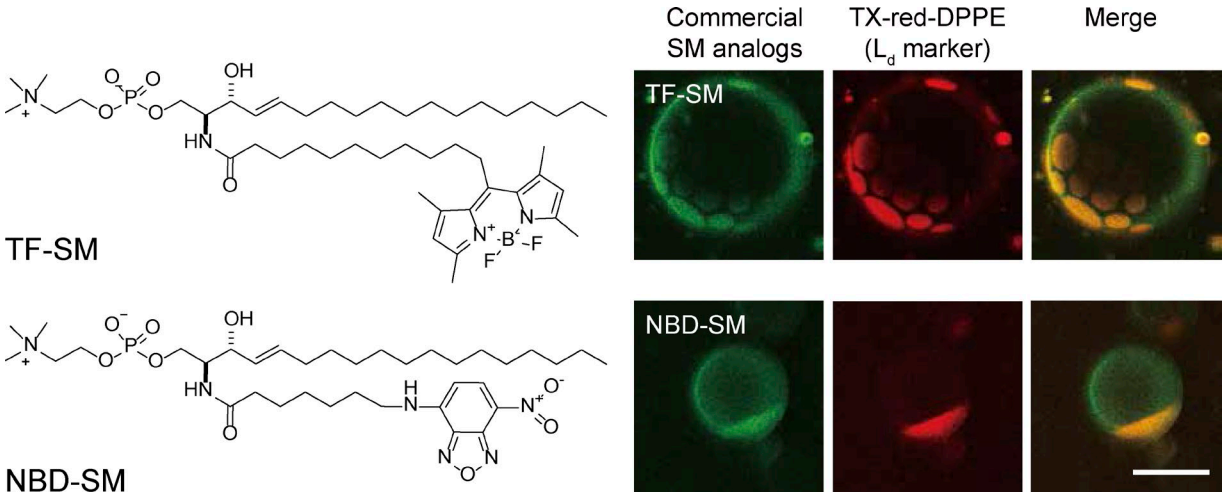

Figure S1. **Commercially available SM analogs.** TopFluor-SM and NBD-SM, which have previously been used as fluorescent SM analogs (McIntosh et al., 2010; Qin and Dawson, 2012), are preferentially partitioned into Ld domains, rather than Lo domains, in Lo-Ld phase–separated GUVs (consisting of equimolar SM[C18:0], DOPC, and cholesterol). Texas-red-DPPE was used as the Ld-domain marker. Bar, 20 µm.

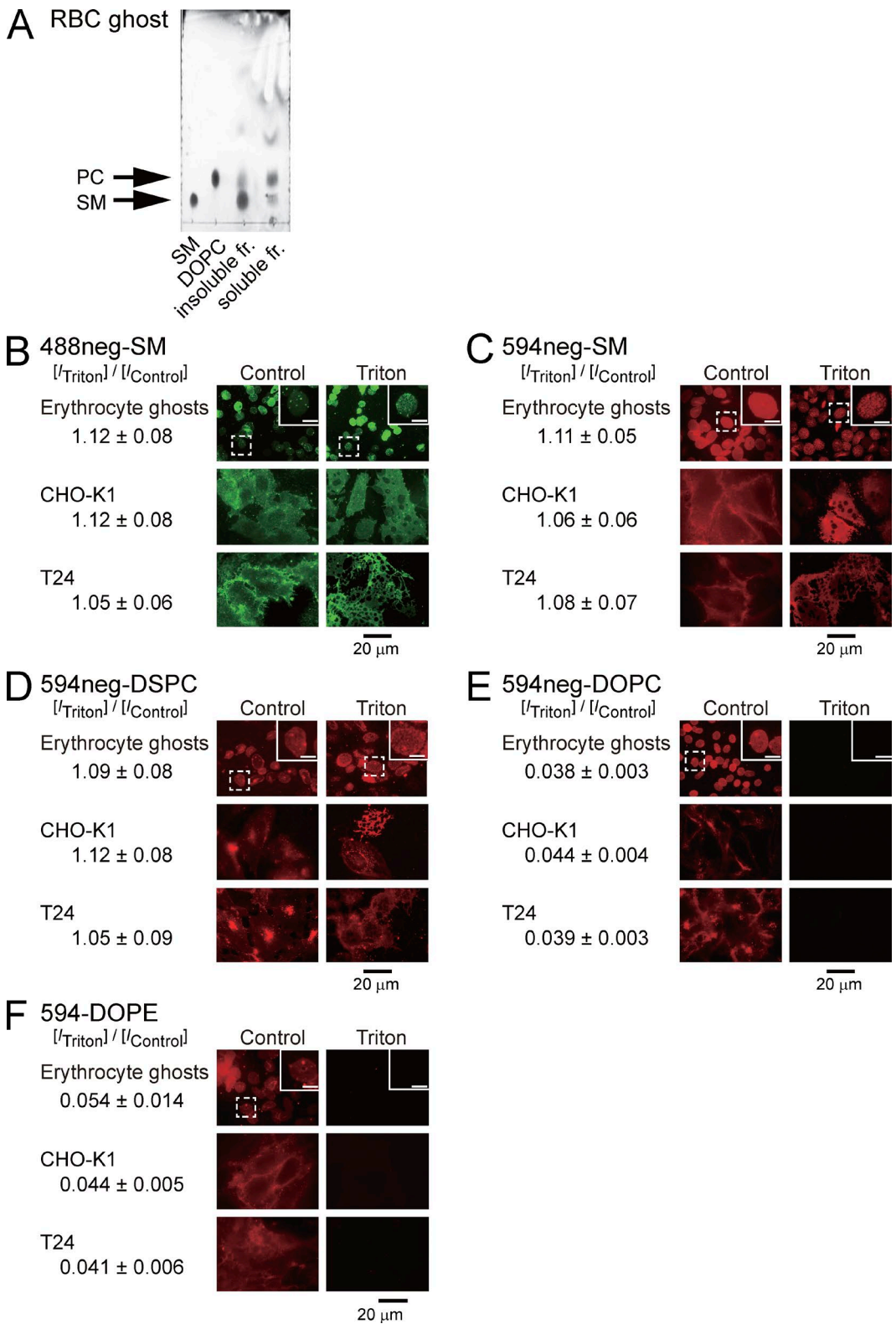

Figure S2. **Cold-Triton (1%; in)solubilities of endogenous SM and PC in human erythrocyte ghosts, and 488neg-SM, 594neg-SM, 594neg-DSPC, 594neg-DOPC, and 594-DOPE preincorporated in human erythrocyte ghosts and the PMs of CHO-K1 and T24 cells.** (A) Endogenous SM and PC in human erythrocyte ghost membranes, detected in 1% cold Triton–soluble and –insoluble fractions (DRMs) by high-performance thin layer chromatography. Standards, SM (C18:0) and DOPC. (B–F) Epifluorescence micrographs of 488neg-SM (B), 594neg-SM (C), 594neg-DSPC (D), 594neg-DOPC (E), and 594-DOPE (F) in DRMs of erythrocyte ghost membranes, CHO-K1-cell PM, and T24-cell PM. Left and right, before and 20 min after cold Triton treatment. The numbers on the left indicate mean ± SE of the ratio of the fluorescence intensities after versus before cold-Triton treatment ($I_{Triton}/I_{Control}$; n = 31–53 cells). Bars: 20 µm; (insets) 5 µm.

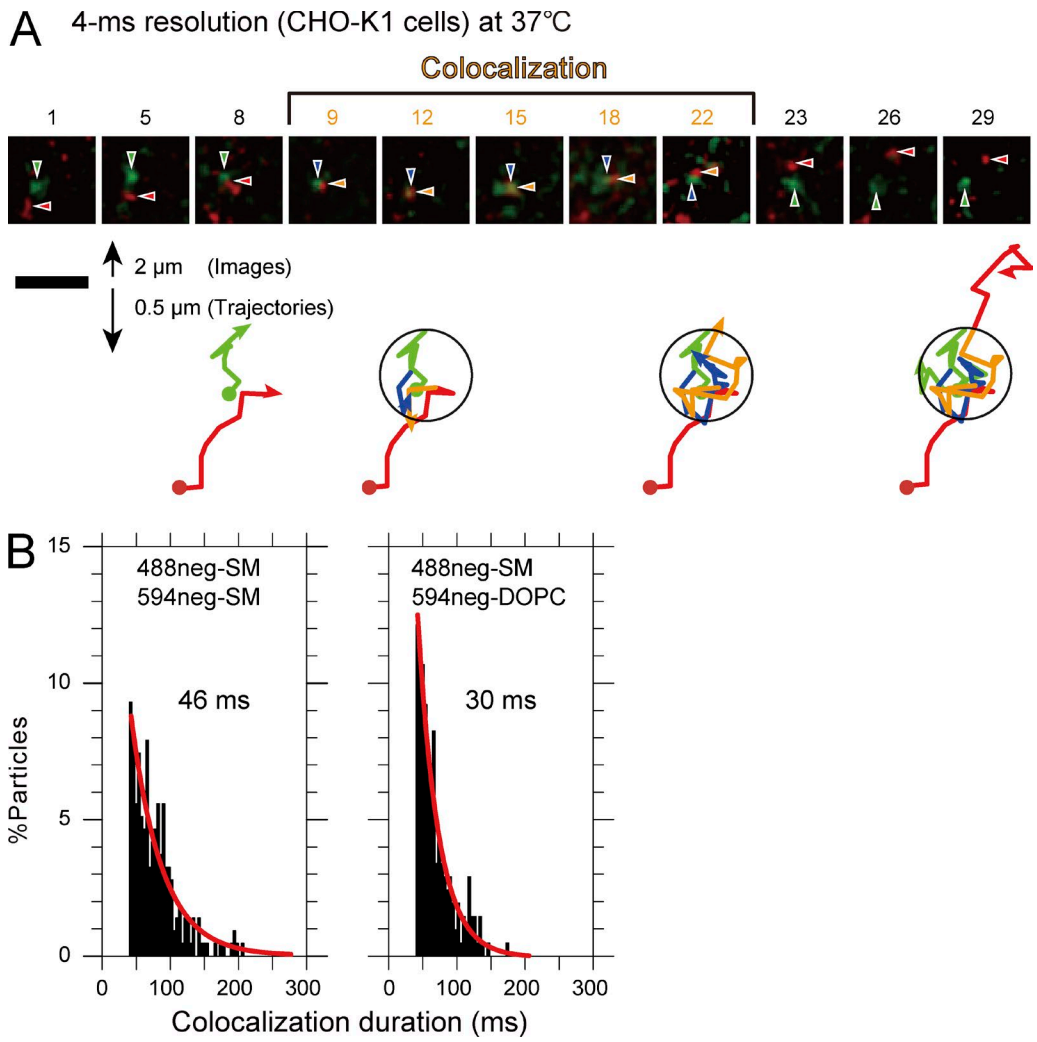

Figure S3. **Simultaneous two-color single-molecule tracking of 488neg-SM and 594neg-SM, as well as single-color single molecule tracking of 594neg-SM, shows prolonged colocalization of SM probes in the CHO-K1-cell PM at 37°C.** (A) Representative simultaneous two-color single-molecule image sequences of 488neg-SM (green) and 594neg-SM (red), observed at a 4-ms resolution (frame rate, 250 Hz). The colocalization of two spots with different colors was determined by measuring the distances between the two determined coordinates. The numbers above the images indicate the number of frames. The trajectory of the 488neg-SM molecule in the images is displayed in green, blue, and green, and the trajectory of the 594neg-SM molecule shown in the images is displayed in red, orange, and red, before, during, and after colocalization, respectively. Bars: (images) 2 μm; (trajectories) 0.5 μm. The initial points of the trajectories are shown by closed circles. The end points of the trajectories shown by the arrowheads match the fluorescent spots indicated by the arrowheads in the image right above the trajectory. (B) Distribution of individual colocalization durations. The colocalization (codiffusion) lifetime was 46 ms (left, n = 214). The experiments for 488neg-SM versus 594neg-DOPC were performed (right, n = 206), but no prolonged colocalization was observed.

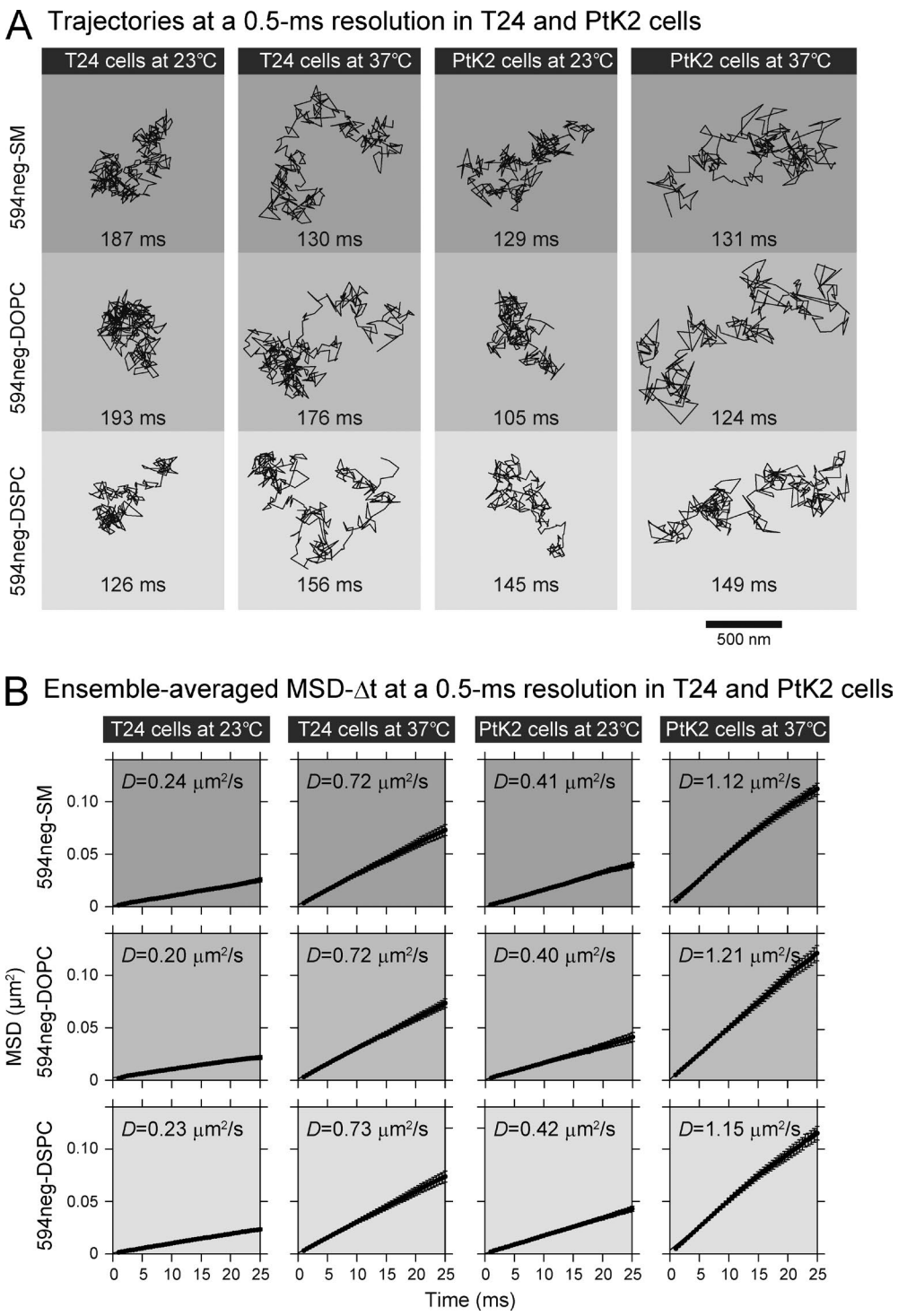

Figure S4. **Diffusion of 594neg-SM, DSPC, and DOPC in the T24- and PtK2-cell PMs at 23°C and 37°C, recorded at a time resolution of 0.5 ms.** (A) Typical trajectories of single 594neg-SM and DOPC molecules in T24- and PtK2-cell PMs at 23°C and 37°C, exhibiting no signs of temporary immobilization. The time (milliseconds) indicates the total duration of the trajectory. Meanwhile, using ATTO647N-SM, Honigmann et al. (2014) previously revealed transient, dynamic molecular interaction hotspots. The interaction sites are smaller than 80 nm in diameter, and ATTO647N-SM was transiently trapped for several milliseconds in these areas. However, the authors themselves had previously shown that this sphingolipid "analog" did not behave like a raft-associated molecule, unlike native sphingolipids (Sevcsik et al., 2015). Therefore, Honigmann et al. (2014) clearly and correctly concluded that the hotspots that ATTO647N-SM detected were unrelated to raft domains because ATTO647N-SM did not behave like native sphingolipids, in terms of its Lo/Ld partitioning in phase-separated GUVs. Namely, the ATTO647N-SM behaviors described by Honigmann et al. (2014) cannot be considered to represent the true behaviors of sphingolipids. (B) MSD-Δt plots of 594neg-SM, 594neg-DSPC, and 594neg-DOPC in T24- and PtK2-cell PMs at 23°C and 37°C (mean ± SE of MSD; *n* is the same as that in Fig. S5). These plots were practically linear between 1 and 25 ms, suggesting that both molecules underwent effective, simple Brownian diffusion on this time scale. The diffusion coefficients for 594neg-SM, 594neg-DSPC, and 594neg-DOPC evaluated from these MSD-Δt plots were indistinguishable from each other, in agreement with the diffusion coefficient distribution obtained for each molecule on the time scale between 1 and 3.5 ms (Fig. S5).

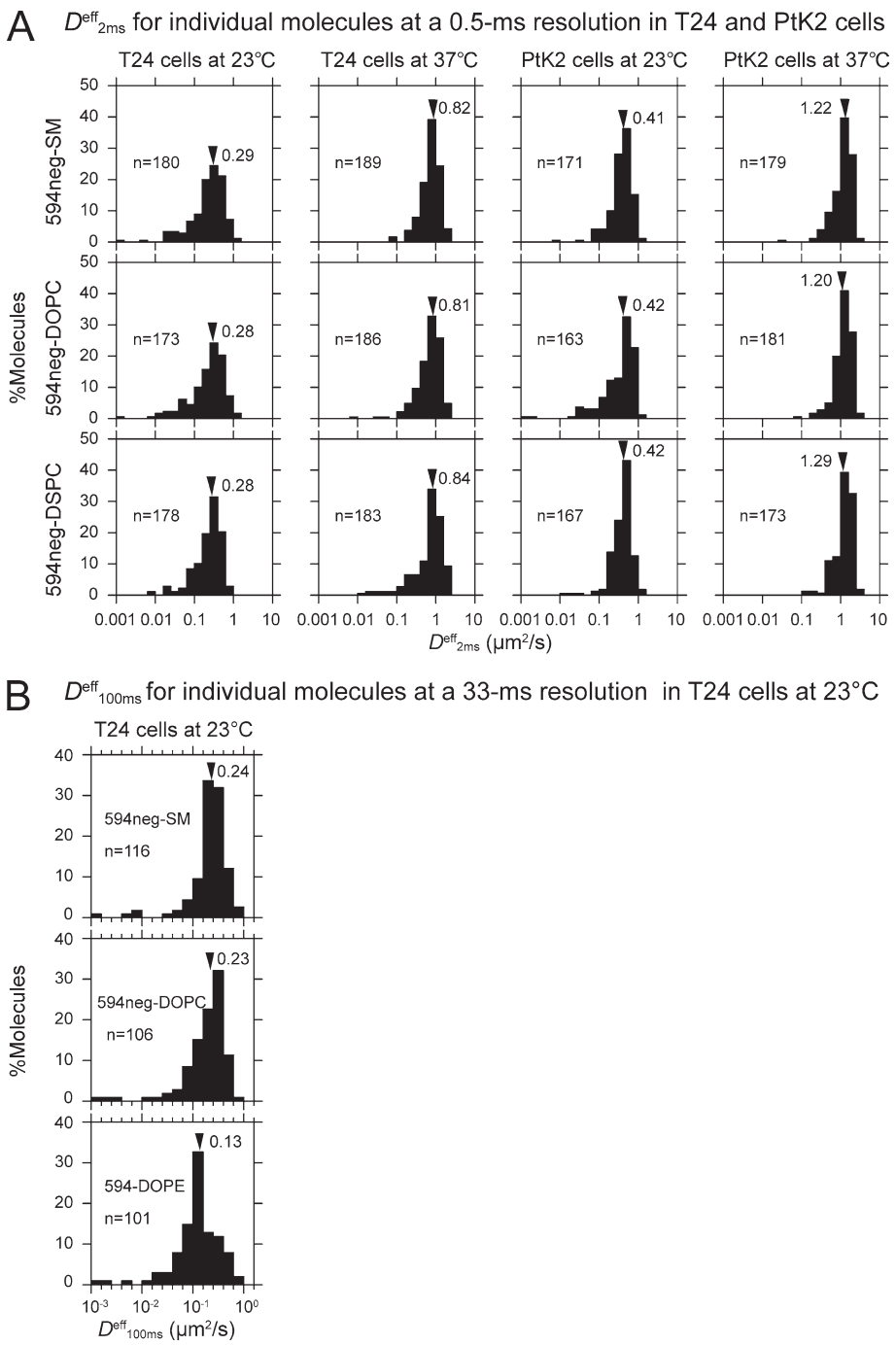

Figure S5. **Distributions of the diffusion coefficients of single molecules of 594neg-SM, 594neg-DOPC, and 594neg-DSPC in the T24- and PtK2-cell PMs at 23°C and 37°C observed in the time windows of 2 and 100 ms, evaluated from trajectories obtained at 0.5- and 33-ms resolutions, respectively.** In contrast to the data shown in Fig. S4 (representing the ensemble-averaged behavior for all molecules observed here), the diffusion coefficient of each individual molecule was determined from each trajectory, and the histogram was generated from these values. Arrowheads indicate median values. (A) D_{2ms} values (determined in the time window between 1 and 3.5 ms), evaluated from trajectories obtained at a 0.5-ms resolution (trajectories longer than 50 steps or 25 ms were used for the analysis). The D_{2ms} values for 594neg-SM, 594neg-DOPC, and 594neg-DSPC in both T24- and PtK2-cell PMs were similar to each other at both 23°C and 37°C. (B) D_{100ms} values (determined in the time window between 67 and 133 ms), obtained in the T24-cell PM at 23°C, evaluated from trajectories obtained at video rate (trajectories longer than 30 steps or 1 s were used for the analysis). The D_{100ms} value for 594neg-SM is similar to that for 594neg-DOPC ($P > 0.4$; *U* test), whereas the D_{100ms} value for 594-DOPE, in which ATTO594 was directly linked to the amine group of the DOPE headgroup without the NEG linker, was significantly smaller ($P < 0.002$; *U* test). The median D_{100ms} values were 0.24 and 0.23 μm²/s for 594neg-SM and 594neg-DOPC, respectively, supporting that 594neg-SM and 594neg-DOPC diffuse at the same rate in the T24-cell PM ($P > 0.4$, *U* test). Interestingly, 594-DOPE, in which the ATTO594 dye was directly conjugated to the amine group of the ethanolamine headgroup without the NEG linker, diffused at a significantly slower rate (median value = 0.13 μm²/s) than that of 594neg-DOPC (median value = 0.23 μm²/s; $P < 0.002$, *U* test). Following the same argument advanced for the SM analogs, 594neg-DOPC might mimic the phospholipid behavior better than 594-DOPE in the PM. Both probes are expected to be in the outer leaflet of the PM, because the diffusion measurements were conducted immediately after the incorporation of the lipid probes to avoid the influence of metabolic changes, and the measurements were conducted at a lower temperature of 23°C. Furthermore, after fluorescent dye conjugation, the DOPE headgroup is quite different from the native phosphorylamine.

Provided online are six tables in a PDF. Table S1 shows the fractions of 594neg-SM, 594neg-DOPC, and 594-DOPE located in the PM inner leaflet. Table S2 shows the lifetimes of homo- and hetero-colocalization of lipid analogs in CHO-K1 cells at 37°C as well as in the Lα- and Lo-phase domains of planar lipid bilayers. Table S3 shows the time fractions of mobile, TALL, and immobile periods for 594neg-SM, 594neg-DOPC, and 594neg-DSPC trajectories obtained at a time resolution of 0.5 ms in the intact PMs of the T24 and PtK2 cell lines. Table S4 shows diffusion coefficients on the time scale of 2.3 ms for 594neg-SM, DOPC, and DSPC in the T24-cell PM and the PtK2-cell PM at 23°C and 37°C. Table S5 shows the colocalization lifetimes of CD59 clusters with 594neg-SM, 594neg-DOPC, and 594neg-DSPC (T24 cells) and those of CD59 transient homodimer rafts and monomers with 594neg-SM and 594neg-DOPC (CHO-K1 cells) at 37°C. Table S6 shows the colocalization lifetimes of FcεRI clusters with 594neg-SM and 594neg-DOPC (RBL-2H3 cells) at 37°C.

References

Honigmann, A., V. Mueller, H. Ta, A. Schoenle, E. Sezgin, S.W. Hell, and C. Eggeling. 2014. Scanning STED-FCS reveals spatiotemporal heterogeneity of lipid interaction in the plasma membrane of living cells. *Nat. Commun.* 5:5412. http://dx.doi.org/10.1038/ncomms6412

McIntosh, A.L., S.M. Storey, and B.P. Atshaves. 2010. Intracellular lipid droplets contain dynamic pools of sphingomyelin: ADRP binds phospholipids with high affinity. *Lipids.* 45:465–477. http://dx.doi.org/10.1007/s11745-010-3424-1

Qin, J., and G. Dawson. 2012. Evidence for coordination of lysosomal (ASMase) and plasma membrane (NSMase2) forms of sphingomyelinase from mutant mice. *FEBS Lett.* 586:4002–4009. http://dx.doi.org/10.1016/j.febslet.2012.09.039

Sevcsik, E., M. Brameshuber, M. Fölser, J. Weghuber, A. Honigmann, and G.J. Schütz. 2015. GPI-anchored proteins do not reside in ordered domains in the live cell plasma membrane. *Nat. Commun.* 6:6969. http://dx.doi.org/10.1038/ncomms7969